condensed matter

MDPI

Article

Ultrafast Pump–Probe Spectroscopy in Organic Dirac Electron Candidate α-$(BETS)_2I_3$

Satoshi Tsuchiya [1,*], Masato Katsumi [1], Ryuhei Oka [2], Toshio Naito [2] and Yasunori Toda [1]

[1] Department of Applied Physics, Hokkaido University, Sapporo 060-8628, Hokkaido, Japan
[2] Graduate School of Science and Engineering, Ehime University, Matsuyama 790-8577, Ehime, Japan
* Correspondence: satoshi.tsuchiya@eng.hokudai.ac.jp

Abstract: Photo-induced carrier dynamics were measured in the organic Dirac electron candidate α-$(BETS)_2I_3$ to investigate why resistivity increases below T_{MI} = 50 K. We found a change in carrier dynamics due to an insulating gap formation below T' = 50 K. On the other hand, the relaxation time and polarization anisotropy of the observed dynamics differ from those in the charge-ordering (CO) state of the isostructural salt α-$(ET)_2I_3$. Based on the difference, it can be concluded that the insulating phase has a different origin than the CO state.

Keywords: organic conductor; Dirac electron system; pump–probe time-resolved spectroscopy

Citation: Tsuchiya, S.; Katsumi, M.; Oka, R.; Naito, T.; Toda, Y. Ultrafast Pump–Probe Spectroscopy in Organic Dirac Electron Candidate α-$(BETS)_2I_3$. *Condens. Matter* **2023**, *8*, 88. https://doi.org/10.3390/condmat8040088

Academic Editors: Antonio Bianconi and Yasutomo Uemura

Received: 31 August 2023
Revised: 14 September 2023
Accepted: 8 October 2023
Published: 10 October 2023

1. Introduction

Organic molecular conductors have been widely studied due to their rich variety of electronic phases due to strong electron correlations [1,2]. Among them, α-$(BETS)_2I_3$ (hereafter α-BETS), where BETS denotes bis(ethylenedithio)tetraselenafulvalene [3,4], has attracted attention as a candidate of the Dirac electron system [5–8], which has a linear energy dispersion in the band structure at ambient pressure, expecting unique electronic properties such as temperature-independent resistivity [9,10]. On the other hand, resistivity gradually increases with a decreasing temperature below T_{MI} = 50 K and a step-like change at around 40 K, and these origins are still controversial [11]. To date, theoretical studies [12,13], as well as various transport and magnetic measurements [14–19], have been conducted to elucidate the rise in resistivity. However, time-resolved spectroscopic measurements are still lacking.

Pump–probe time-resolved spectroscopy using femtosecond optical pulses has often been used to study the electronic properties of strongly correlated electron systems. In time-resolved spectroscopy, even if an electron system is perturbed by light on a large energy scale, the carrier relaxation process allows us to indirectly observe the electronic state as if it were unperturbed (not excited), and to capture small energy gaps and anisotropy. In fact, in organic conductors, this method has been utilized to study correlation-induced insulating states [20,21], and has contributed to elucidating their electronic properties. Thus, by measuring the carrier dynamics in α-BETS, we can gain new insights into the origin of the increase in resistivity at low temperatures.

In this paper, photo-induced carrier relaxation dynamics in α-BETS are reported. The signal amplitude of the dynamics begins to increase at T' = 50 K, which agrees with T_{MI}, indicating the formation of an energy gap. Moreover, the gap amplitude estimated from the fitting analysis almost agrees with that estimated from the resistivity measurements. On the other hand, the observed dynamics are different from that in a charge-ordering (CO) state of the isostructural salt α-$(ET)_2I_3$ (hereafter α-ET), where ET denotes bis(ethylenedithio)-thiotetrathiafulvalene, with respect to relaxation time and polarization anisotropy. Therefore, the origin of the resistivity increase is likely to be an insulating phase different from the CO states.

2. Materials and Methods

Single crystals of α-BETS were synthesized electrochemically [3]. Figure 1a shows schematic illustrations of BETS and ET molecules. The crystal consists of an alternating structure of conducting layer of BETS molecules and an insulating layer of I_3. As shown in Figure 1b, BETS molecules are arranged and form a conducting layer.

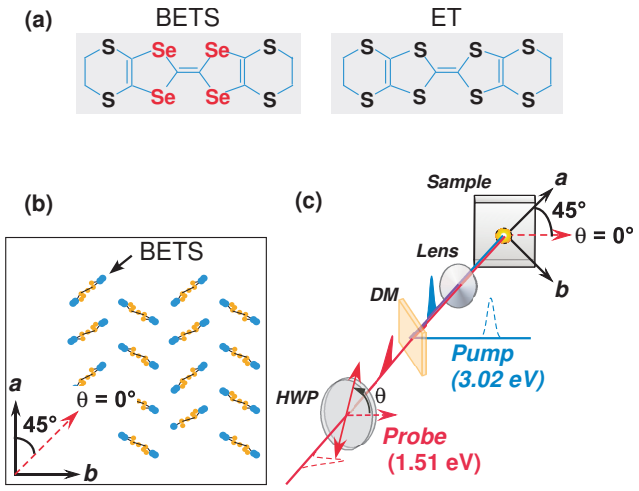

Figure 1. (**a**) Schematic illustrations of BETS and ET molecules. S and Se stand for sulfur and selenium atoms. (**b**) A schematic illustration of an arrangement of BETS molecules in α-BETS. The blue and orange balls denote sulfur and carbon atoms. (**c**) A schematic view of the measurement setup for pump–probe spectroscopy. DM and HWP represent a dichroic mirror and a half-wave plate, respectively. Some figures are reused from those used in the recent paper [22].

Figure 1c shows the schematic view of the setup for a pump–probe measurement. The measurements were made with 120 fs laser pulses centered at 1.51 eV obtained from a cavity-dumped mode-lock Ti:sapphire oscillator. A repetition rate was set as 54 kHz to avoid the heating effect. Pulses were separated into two paths; one was used for a probe, while the other was changed to pulses centered at 3.02 eV by a standard frequency doubling for a pump. The pump and probe beams were superimposed on the same axis and incident perpendicular to the conduction (***ab***) plane of the sample. The polarization of the probe was changed by rotating the half-wave plate, and the polarization angle was measured from a direction tilted 45 degrees from the ***a*** axis. The spot sizes of the pump and probe beams were $\sim$20 μm and $\sim$12 μm in diameter, respectively.

In pump–probe measurement, after excitation by the pump pulse, the carriers relax immediately and accumulate in electronic states near the Fermi energy, forming the non-equilibrium occupation of carriers as well as phonons [23]. In the subsequent probing process, the non-equilibrium carrier distribution is measured as a transient change in reflectivity ($\Delta R/R$). When a gap for a low-energy electronic excitation such as an insulating gap is formed at low temperatures, a relaxation bottleneck occurs [24,25], leading to significant changes in $\Delta R/R$, such as an increase or decrease in the signal amplitude and long relaxation. Therefore, the gap formation can be probed by measuring the temperature dependence. Moreover, by measuring probe polarization dependence, we can obtain information on the anisotropic ordering of electrons, such as the CO state [21,22]. The data were taken with increasing temperature with the pump fluence of $F = 59$ μJ/cm^2.

3. Results

Figure 2a,b show the transient change of reflectivity ($\Delta R/R$) from $\theta = 0°$, 45° (***a*** axis), 90°, 135° (***b*** axis), 180°, 225° (***a*** axis), 270°, 315° (***b*** axis), and 360° at $T = 20$ K and 120 K, respectively. At $T = 120$ K, $\Delta R/R$ changes depend on θ. When the temperature changes from 120 K to 20 K, the signal amplitude increases for all values of θ. Figure 2c,d show

the polar plots of the signal amplitude at T = 20 K and 120 K, respectively. At T = 120 K, the signal is enhanced in the b axis direction, the trend of which does not change at T = 20 K.

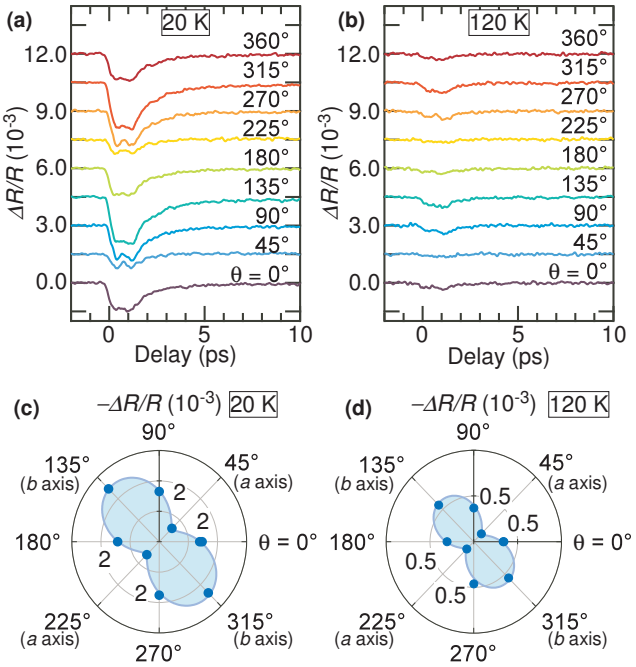

Figure 2. (**a**,**b**) Transient change in reflectivity ($\Delta R/R$) from $\theta = 0°$ to 360° by 45° steps at T = 20 K and 120 K, respectively. The data are shifted for clarity. (**c**,**d**) Polar plots of the amplitude of $\Delta R/R$ as a function of θ at T = 20 K and 120 K, respectively. The signal amplitude is the $\Delta R/R$ value at 1 ps. The solid lines denote the results fitted using Equation (1).

To decompose the transient data into polarization-dependent (anisotropic) and -independent (isotropic) dynamics, we tried the following analyses. Since the probe beam is linearly polarized, $\Delta R/R$ is a function of θ with a period of 180°. The data are fitted using the following equation:

$$\frac{\Delta R}{R}(\theta) = \frac{\Delta R_{\mathrm{iso}}}{R} + \frac{\Delta R_{\mathrm{ani}}}{R}\cos(2\theta - 2\theta_0), \tag{1}$$

where $\Delta R_{\mathrm{ani}}/R$ and $\Delta R_{\mathrm{iso}}/R$ are anisotropic and isotropic transients, respectively, and θ_0 is a phase corresponding to a direction wherein the transient signal is most enhanced. If the CO state appears, polarization dependence will change across the transition temperature. Even in that case, this analysis can characterize the anisotropy of the CO state as a change in θ_0 [22]. Figure 3a,b show $\Delta R_{\mathrm{ani}}/R$ and $\Delta R_{\mathrm{iso}}/R$, respectively, for T = 20, 40, 80, 120, and 150 K. When the temperature decreases, the negative signal seems to increase in both components. We note that the double peak structure observed before ∼1.5 ps of the isotropic component is attributed to the oscillatory component. However, its origin is beyond the scope of this paper and is not discussed further.

To discuss the temperature dependencies in more detail, the data are fitted with a single exponential function

$$\frac{\Delta R_{\mathrm{ani}}}{R}(t) = A_{\mathrm{ani}}\exp(-t/\tau_{\mathrm{ani}}) + C_{\mathrm{ani}} \tag{2}$$

for the anisotropic component or

$$\frac{\Delta R_{\mathrm{iso}}}{R}(t) = A_{\mathrm{iso}}\exp(-t/\tau_{\mathrm{iso}}) + C_{\mathrm{iso}}, \tag{3}$$

for the isotropic component, where A_{ani}, A_{iso} and τ_{ani}, τ_{iso} are the amplitude and relaxation time of a short-lived component. C_{ani} and C_{iso} are the amplitude of long-lived component when its relaxation time is assumed to be infinite. Figure 4a shows the temperature dependencies of the absolute values of A_{ani} and C_{ani}. As temperature decreases, $|A_{ani}|$ increases below $T' = 50$ K, which agrees with T_{MI}. On the other hand, the temperature dependence of $|C_{ani}|$ shows little change. Moreover, the τ_{ani} values gradually reach ∼1.5 ps at low temperatures and show no significant change around T', as shown in Figure 4b. Figure 4c shows the temperature dependence of θ_0 at a delay of 1 ps. The θ_0 values are ∼135° in the whole temperature range, indicating no anisotropic electronic ordering below T'.

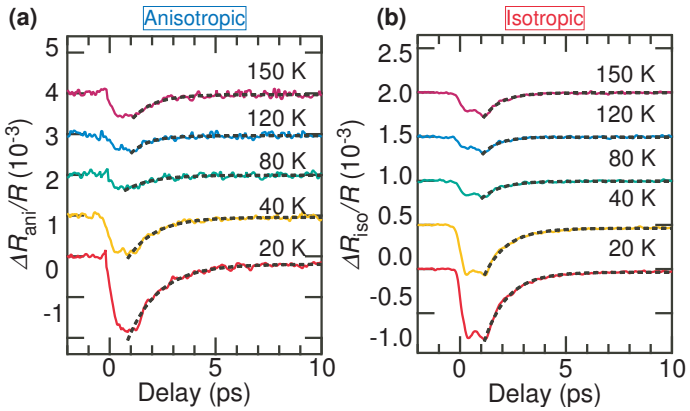

Figure 3. (**a**,**b**) $\Delta R_{ani}/R$ and $\Delta R_{iso}/R$, respectively, for T = 20, 40, 80, 120, and 150 K. The dashed lines are the results obtained by fitting with the single exponential function. The data are vertically offset for clarity.

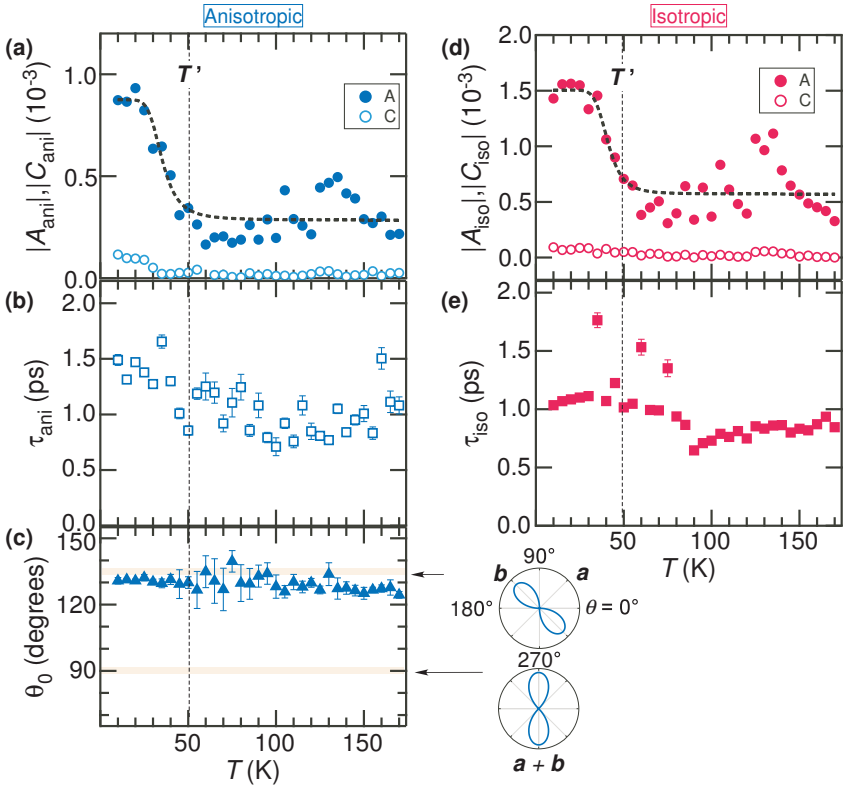

Figure 4. (**a**) Temperature dependencies of $|A_{ani}|$ and $|C_{ani}|$. The dashed line is the fitting results using Equation (4). (**b**) Temperature dependence of the relaxation time τ_{ani}. (**c**) Temperature dependence of θ_0. Temperature dependencies of $|A_{iso}|$ and $|C_{iso}|$ (**d**) and τ_{iso} (**e**). T' is the temperature at which $|A|$ changes suddenly and drastically with decreasing temperature.

In the isotropic component, the temperature dependencies of $|A_{iso}|$ and τ_{iso} are similar to those in the anisotropic component. The similarity between the anisotropic and isotropic dynamics suggests that they have the same origin. We note a broad peak structure in the temperature dependencies of A_{ani} and A_{iso} at high temperatures, as shown in Figure 4a,d. This is due to a change in beam irradiation position with temperature variation and is not intrinsic.

Since the observed changes in $|A_{ani}|$ and $|A_{iso}|$ reflect the changes in non-equilibrium carrier distribution, information on the gap magnitude can be extracted from the temperature dependencies of $|A_{ani}|$ and $|A_{iso}|$. The gap (Δ_{gap}) can be estimated by fitting with a temperature-independent gap model, which is often used in the gradual temperature dependence in the amplitude (A) such as pseudogap response in cuprate superconductors [25]. In the model, the amplitude is written as

$$A(T) \propto \left[1 + b \exp\left(-\frac{\Delta_{gap}}{k_B T}\right)\right]^{-1}, \quad (4)$$

where b, and k_B are variable parameters for the fit and the Boltzmann constant, respectively. As shown by the dashed lines in Figure 4a,d, the data are fitted well, and the gap is estimated as $\Delta_{gap} \approx 24$ meV and 35 meV for the anisotropic and the isotropic components, respectively, which agree with that estimated from the analysis of the Arrhenius plot in the resistivity measurements. Therefore, the results indicate that a band gap opens at $T' = 50$ K in the α-BETS.

4. Discussion

Here, possible origins of the observed dynamics below T' are discussed through comparison with the isostructural salt α-ET, which undergoes a CO transition at $T_{co} = 135$ K [26–30]. The CO state is characterized by three features of photoinduced carrier dynamics [22]. The first one is the signal amplitude, which begins to change at around T_{co}, and the change is explained by the insulating gap formation due to the CO. Secondly, a divergent behavior of the relaxation time is observed just below T_{co}. This behavior is attributed to a phonon-bottleneck effect [25] due to critical fluctuation related to long-range electronic ordering just below T_{co}. Thirdly, θ_0 changes to 90° where the transient signal is most enhanced along the $\frac{1}{2}(\boldsymbol{a} + \boldsymbol{b})$ axis, below T_{co}. This polarization anisotropy indicates an anisotropic ordering of electrons [31–33], consistent with the CO state.

In α-BETS, the signal amplitude increases below $T' = 50$ K, which is similar to α-ET. Considering the consistency between the pump–probe and resistivity measurements, this behavior can be attributed to the formation of an insulating gap. However, in contrast to α-ET, there are no significant changes in τ_{ani}, τ_{iso} and θ_0 at T'. The difference between α-BETS and α-ET suggests that the origin of the resistivity increase below T' differs from the CO state.

One of the possible origins of this is topological insulators (TIs), which generally have an insulator-type band gap in the bulk but have a gapless conducting phase on their surface. As shown in Figure 1a, the BETS molecule is obtained by replacing four inner sulfur atoms of the ET molecule with selenium atoms. Due to the fact that a spin-orbit coupling (SOC) increases with the selenium substitution, the SOC in α-BETS can be more significant than in α-ET. Indeed, a recent theoretical study has suggested that SOC induces a gap, leading to a weak topological insulator [7]. Moreover, electron correlation is also crucial for the emergence of the topological phase [12,13], and anomalous transport properties originating from correlation-induced topological insulators have been observed experimentally [19]. We comment on the difficulty to refer to the relation between the electron correlation anisotropy and the polarization anisotropy in $\Delta R/R$. The previous study indicated that the charge gap formation is due to the development of one-dimensional anisotropy of spin correlations [13]. However, it is difficult to refer to the relation because the polarization anisotropy in $\Delta R/R$ is a consequence of the anisotropy regarding the optical transitions after the pump irradiation and is not directly related to the low-energy electronic gap

structure [21].

In TI states, there is no anisotropy due to charge disproportionation. This means that the dynamics of the state are expected to stay constant with the relaxation time and θ_0, and only the amplitude is likely to vary due to the bulk gap. These predictions are consistent with the present results, suggesting that the dynamics observed below $T' = 50$ K could be due to the insulator gap as a bulk property of TI. It is also worth noting that the present results do not show any anomaly in dynamics at around 40 K, where the resistivity shows a step-like change [11]. The recent study has suggested a crossover from two-dimensional to three-dimensional TI at ∼35 K [19], resulting in a change in the conducting surface states. Therefore, during the crossover, the bulk band gap is not affected, which is consistent with the lack of change in dynamics. In general, it is difficult to distinguish between the carrier dynamics arising from the bulk state and those from the surface state. Thus, other measurements, such as a spectrally resolved pump–probe measurements, may be needed to clarify the contribution from the surface.

5. Conclusions

Through pump–probe time-resolved spectroscopy, the photo-induced carrier dynamics were found to change below $T' = 50$ K. This finding corresponds to the increase in resistivity. Compared with α-ET, the observed dynamics below T' differ from those in the CO state regarding relaxation time and polarization anisotropy, but they are compatible with those predicted in the TI.

Author Contributions: S.T., M.K. and Y.T. performed the optical pump–probe measurements. R.O. and T.N. prepared organic crystals. S.T. prepared manuscripts based on the discussions with all co-authors. All authors have read and agreed to the published version of the manuscript.

Funding: This research was funded by JSPS KAKENHI Grants No. JP22H01162.

Data Availability Statement: All the data suggested in this study are available from the corresponding author (S.T.) upon reasonable request.

Acknowledgments: The authors acknowledge N. Kanai for experimental support and helpful discussions.

Conflicts of Interest: The authors declare no conflict of interest.

References

1. Ardavan, A.; Brown, S.; Kagoshima, S.; Kanoda, K.; Kuroki, K.; Mori, H.; Ogata, M.; Uji, S.; Wosnitza, J. Recent Topics of Organic Superconductors. *J. Phys. Soc. Jpn.* **2012**, *81*, 011004. [CrossRef]
2. Naito, T. Modern History of Organic Conductors: An Overview. *Crystals* **2021**, *11*, 838. [CrossRef]
3. Kato, R.; Kobayashi, H.; Kobayashi, A. Synthesis and properties of bis(ethylenedithio)tetraselenafulvalene (BEDT-TSeF) compounds. *Synth. Met.* **1991**, *42*, 2093–2096. [CrossRef]
4. Kondo, R.; Kagoshima, S.; Tajima, N.; Kato, R. Crystal and Electronic Structures of the Quasi-Two-Dimensional Organic Conductor α-(BEDT-TTF)2I3 and Its Selenium Analogue α-(BEDT-TSeF)2I3 under Hydrostatic Pressure at Room Temperature. *J. Phys. Soc. Jpn.* **2009**, *78*, 114714. [CrossRef]
5. Morinari, T.; Suzumura, Y. On the Possible Zero-Gap State in Organic Conductor α-(BEDT-TSF)2I3 under Pressure. *J. Phys. Soc. Jpn.* **2014**, *83*, 094701. [CrossRef]
6. Tsumuraya, T.; Suzumura, Y. First-principles study of the effective Hamiltonian for Dirac fermions with spin-orbit coupling in two-dimensional molecular conductor α-$(BETS)_2I_3$. *Eur. Phys. J. B* **2021**, *94*, 17. [CrossRef]
7. Kitou, S.; Tsumuraya, T.; Sawahata, H.; Ishii, F.; Hiraki, K.i.; Nakamura, T.; Katayama, N.; Sawa, H. Ambient-pressure Dirac electron system in the quasi-two-dimensional molecular conductor $\alpha-(BETS)_2I_3$. *Phys. Rev. B* **2021**, *103*, 035135. [CrossRef]
8. Oka, R.; Ohara, K.; Konishi, K.; Yamane, I.; Shimada, T.; Naito, T. Band Structure Evolution during Reversible Interconversion between Dirac and Standard Fermions in Organic Charge-Transfer Salts. *Magnetochemistry* **2023**, *9*, 153. [CrossRef]
9. Shon, N.H.; Ando, T. Quantum Transport in Two-Dimensional Graphite System. *J. Phys. Soc. Jpn.* **1998**, *67*, 2421–2429. [CrossRef]
10. Tajima, N.; Sugawara, S.; Tamura, M.; Nishio, Y.; Kajita, K. Electronic Phases in an Organic Conductor α-$(BEDT\text{-}TTF)_2I_3$: Ultra Narrow Gap Semiconductor, Superconductor, Metal, and Charge-Ordered Insulator. *J. Phys. Soc. Jpn.* **2006**, *75*, 051010. [CrossRef]
11. Inokuchi, M.; Tajima, H.; Kobayashi, A.; Ohta, T.; Kuroda, H.; Kato, R.; Naito, T.; Kobayashi, H. Electrical and Optical Properties of α-$(BETS)_2I_3$ and α-$(BEDT\text{-}STF)_2I_3$. *Bull. Chem. Soc. Jpn.* **1995**, *68*, 547–553. [CrossRef]

12. Ohki, D.; Yoshimi, K.; Kobayashi, A. Interaction-induced quantum spin Hall insulator in the organic Dirac electron system α-(BEDT-TSeF)$_2$I$_3$. *Phys. Rev. B* **2022**, *105*, 205123. [CrossRef]
13. Ohki, D.; Yoshimi, K.; Kobayashi, A.; Misawa, T. Gap opening mechanism for correlated Dirac electrons in organic compounds α-(BEDT-TTF)$_2$I$_3$ and α-(BEDT-TSeF)$_2$I$_3$. *Phys. Rev. B* **2023**, *107*, L041108. [CrossRef]
14. Hiraki, K.i.; Harada, S.; Arai, K.; Takano, Y.; Takahashi, T.; Tajima, N.; Kato, R.; Naito, T. Local Spin Susceptibility of α-D2I3 (D = bis(ethylendithio)tetraselenafulvalene (BETS) and bis(ethylendithio)dithiadiselenafulvalene (BEDT-STF)) Studied by 77Se NMR. *J. Phys. Soc. Jpn.* **2011**, *80*, 014715. [CrossRef]
15. Kodama, K.; Nakamura, T.; Takahashi, T.; Ojima, E.; Kobayashi, H. Metal-insulator transition in α-(BEDT-TSeF)2I3 and α-(BEDT-TTF)2I3. *Synth. Met.* **1999**, *103*, 1963–1964. [CrossRef]
16. Kawasugi, Y.; Masuda, H.; Uebe, M.; Yamamoto, H.M.; Kato, R.; Nishio, Y.; Tajima, N. Pressure-induced phase switching of Shubnikov–de Haas oscillations in the molecular Dirac fermion system α-(BETS)$_2$I$_3$. *Phys. Rev. B* **2021**, *103*, 205140. [CrossRef]
17. Fujiyama, S.; Maebashi, H.; Tajima, N.; Tsumuraya, T.; Cui, H.B.; Ogata, M.; Kato, R. Large Diamagnetism and Electromagnetic Duality in Two-Dimensional Dirac Electron System. *Phys. Rev. Lett.* **2022**, *128*, 027201. [CrossRef]
18. Konoike, T.; Terashima, T.; Uji, S.; Hattori, Y.; Kato, R. Magnetic Order in Organic Dirac Electron System α-(BETS)2I3. *J. Phys. Soc. Jpn.* **2022**, *91*, 043703. [CrossRef]
19. Nomoto, T.; Imajo, S.; Akutsu, H.; Nakazawa, Y.; Kohama, Y. Correlation-driven organic 3D topological insulator with relativistic fermions. *Nat. Commun.* **2023**, *14*, 2130. [CrossRef]
20. Tsuchiya, S.; Nakagawa, K.; Taniguchi, H.; Toda, Y. Polarization-resolved Ultrafast Spectroscopy in an Organic Mott Insulator κ-(BEDT-TTF)$_2$Cu[N(CN)$_2$]Cl. *J. Phys. Soc. Jpn.* **2019**, *88*, 074706. [CrossRef]
21. Nakagawa, K.; Tsuchiya, S.; Taniguchi, H.; Toda, Y. Probing uniform and nonuniform charge ordering with polarized femtosecond optical pulses in geometrically frustrated θ-(BEDT-TTF)$_2$$M$Zn(SCN)$_4$ (M = Rb, Cs). *Phys. Rev. Res.* **2023**, *5*, 013024. [CrossRef]
22. Tsuchiya, S.; Kanai, N.; Oka, R.; Naito, T.; Toda, Y. Effects of Molecular Substitution in Organic Conductors α-(ET)2I3 and α-(STF)2I3 Studied by Polarized Femtosecond Spectroscopy. *J. Phys. Soc. Jpn.* **2023**, *92*, 094703. [CrossRef]
23. Allen, P.B. Theory of thermal relaxation of electrons in metals. *Phys. Rev. Lett.* **1987**, *59*, 1460–1463. [CrossRef] [PubMed]
24. Rothwarf, A.; Taylor, B.N. Measurement of Recombination Lifetimes in Superconductors. *Phys. Rev. Lett.* **1967**, *19*, 27–30. [CrossRef]
25. Kabanov, V.V.; Demsar, J.; Podobnik, B.; Mihailovic, D. Quasiparticle relaxation dynamics in superconductors with different gap structures: Theory and experiments on YBa$_2$Cu$_3$O$_{7-\mathrm{ffi}}$. *Phys. Rev. B* **1999**, *59*, 1497–1506. [CrossRef]
26. Bender, K.; Hennig, I.; Schweitzer, D.; Dietz, K.; Endres, H.; Keller, H.J. Synthesis, Structure and Physical Properties of a Two-Dimensional Organic Metal, Di[bis(ethylenedithiolo)tetrathiofulvalene] triiodide, (BEDT-TTF)$^+{}_2$I$_3$. *Mol. Cryst. Liq. Cryst.* **1984**, *108*, 359–371. [CrossRef]
27. Takano, Y.; Hiraki, K.; Yamamoto, H.; Nakamura, T.; Takahashi, T. Charge disproportionation in the organic conductor, α-(BEDT-TTF)$_2$I$_3$. *J. Phys. Chem. Solids* **2001**, *62*, 393–395. [CrossRef]
28. S. Moroto.; K.-I. Hiraki.; Y. Takano.; Y. Kubo.; T. Takahashi.; H.M. Yamamoto.; T. Nakamura. Charge disproportionation in the metallic state of α-(BEDT-TTF)$_2$I$_3$. *J. Phys. IV Fr.* **2004**, *114*, 399. [CrossRef]
29. Takahashi, T.; Nogami, Y.; Yakushi, K. Charge Ordering in Organic Conductors. *J. Phys. Soc. Jpn.* **2006**, *75*, 051008. [CrossRef]
30. Yamamoto, K.; Iwai, S.; Boyko, S.; Kashiwazaki, A.; Hiramatsu, F.; Okabe, C.; Nishi, N.; Yakushi, K. Strong Optical Nonlinearity and its Ultrafast Response Associated with Electron Ferroelectricity in an Organic Conductor. *J. Phys. Soc. Jpn.* **2008**, *77*, 074709. [CrossRef]
31. Dvorsek, D.; Kabanov, V.V.; Demsar, J.; Kazakov, S.M.; Karpinski, J.; Mihailovic, D. Femtosecond quasiparticle relaxation dynamics and probe polarization anisotropy in YSr$_x$Ba$_{2-x}$Cu$_4$O$_8$ (x = 0, 0.4). *Phys. Rev. B* **2002**, *66*, 020510. [CrossRef]
32. Toda, Y.; Kawanokami, F.; Kurosawa, T.; Oda, M.; Madan, I.; Mertelj, T.; Kabanov, V.V.; Mihailovic, D. Rotational symmetry breaking in Bi$_2$Sr$_2$CaCu$_2$O$_{8+\delta}$ probed by polarized femtosecond spectroscopy. *Phys. Rev. B* **2014**, *90*, 094513. [CrossRef]
33. Tsuchiya, S.; Sugawara, Y.; Tanda, S.; Toda, Y. Symmetry-dependent carrier relaxation dynamics and charge–density–wave transition in DyTe3 probed by polarized femtosecond spectroscopy. *J. Opt.* **2015**, *17*, 085501. [CrossRef]